8-2009

Rephasing Ion Packets in the Orbitrap Mass Analyzer to Improve Resolution and Peak Shape

Richard H. Perry
Purdue University, rp1195@nova.edu

Qizhi Hu
Amgen Inc.

Gary A. Salazar
Purdue University

R. Graham Cooks
Purdue University

Robert J. Noll
Purdue University

Rephasing Ion Packets in the Orbitrap Mass Analyzer to Improve Resolution and Peak Shape*

Richard H. Perry,[a] Qizhi Hu,[b] Gary A. Salazar,[a] R. Graham Cooks,[a] and Robert J. Noll[a]

[a] Department of Chemistry, Purdue University, West Lafayette, Indiana, USA
[b] Amgen Inc., Thousand Oaks, California, USA

A method is described to improve resolution and peak shape in the Orbitrap under certain experimental conditions. In these experiments, an asymmetric anharmonic axial potential was first produced in the Orbitrap by detuning the voltage on the compensator electrode, which results in broad and multiply split mass spectral peaks. An AC waveform applied to the outer electrode, 180° out of phase with ion axial motion and resonant with the frequency of ion axial motion, caused ions of a given m/z to be de-excited to the equator ($z = 0$) and then immediately re-excited. This process, termed "rephasing," leaves the ion packet with a narrower axial spatial extent and frequency distribution. For example, when the Orbitrap axial potential is thus anharmonically de-tuned, a resolution of 124,000 to 171,000 is obtained, a 2- to 3-fold improvement over the resolution of 40,000 to 60,000 without rephasing, at 10 ng/μL reserpine concentration. Such a rephasing capability may ultimately prove useful in implementing tandem mass spectrometry (MS/MS) in the Orbitrap, bringing the Orbitrap's high mass accuracy and resolution to bear on both the precursor and product ions in the same MS/MS scan and making available the collision energy regime of the Orbitrap, ~1500 eV. (J Am Soc Mass Spectrom 2009, 20, 1397–1404) © 2009 American Society for Mass Spectrometry

Since its introduction, the LTQ-Orbitrap (Thermo Fisher Scientific, San Jose, CA) [1–4] has proven to be a valuable analytical tool with a wide range of applications. Its high resolving power (100,000 at m/z 400) and mass accuracy (2–5 ppm for internal and external calibration, respectively; as low as 0.2 ppm under favorable conditions) [5] significantly reduces false positive peptide identifications in bottom-up [6–8] protein analyses [9, 10] and also improves the accuracy of de novo interpretations [11, 12] of tandem mass spectrometry (MS/MS) data [13, 14]. Up until the introduction of the LTQ-Orbitrap, only Fourier transform ion cyclotron (FT-ICR) mass analyzers had sufficient resolving power and mass accuracy to efficiently characterize intact proteins and their associated fragments. Recent studies have demonstrated that the LTQ-Orbitrap can resolve the isotopic distribution of multiply-charged intact proteins and peptides [15–17], making it an alternative to FT-ICR for top-down [18–20] proteomics. The LTQ-Orbitrap has also found applications in many other scientific research areas such as metabolomics [21], lipidomics [22], and environmental chemistry [23].

The Orbitrap mass analyzer [4, 24–26] is composed of a spindle-like central electrode and a barrel-like outer electrode. A DC voltage is applied between these two specially shaped electrodes, resulting in the following potential distribution:

$$U(r,z) = \frac{k}{2}\left(z^2 - \frac{r^2}{2}\right) + \frac{k}{2}(R_m)^2 \ln\left[\frac{r}{R_m}\right] + C \quad (1)$$

where r and z are cylindrical coordinates, R_m is the characteristic radius, k is the proportionality constant for the axial restoring force and C is a constant [26]. Stable ion trajectories involve both orbiting motion (r, φ-motion, where φ is the angular coordinate) around the central electrode when $r < R_m$ and simultaneous oscillations in the z-direction. The mass-to-charge ratio (m/z) is derived from the natural frequency of oscillation along the z-axis (f), given by the well-known harmonic oscillator relation,

$$\omega = (kq/m)^{1/2} \quad (2)$$

where m and q are the mass and charge of the ion, respectively, and $\omega = 2\pi f$ is the angular frequency in rad/s [26].

* Dedicated to Dr. Alexander Makarov, for the invention of the Orbitrap and his achievements leading to the ASMS Distinguished Contribution to Mass Spectrometry Award.

Address reprint requests to Dr. R. J. Noll, Department of Chemistry, Purdue University, 560 Oval Drive, West Lafayette, IN 47907, USA. E-mail: rnoll@purdue.edu

1044-0305/09/$32.00
doi:10.1016/j.jasms.2009.02.011

Published online February 12, 2009
Received December 14, 2008
Revised February 5, 2009
Accepted February 6, 2009

The image current induced in the outer electrodes (which is split at $z = 0$) by ion axial motion is acquired as a time-domain transient and Fourier-transformed to produce a frequency spectrum [27–30]. Frequencies are converted to m/z by eq 2. The magnitude of the image current produced by N ions with angular frequency ω, axial amplitude Δz and average radius r is given by

$$I(t, r) \approx -qN\omega\frac{\Delta z}{\lambda(r)}\sin(\omega t) \quad (3)$$

The quantity $\lambda(r)$ accounts for the geometry of the Orbitrap electrodes and is a monotonically decreasing function of r [26]. Although radial, angular, and axial frequencies all depend on the m/z ratio, only the axial frequency is used because only this frequency is independent of the initial kinetic energy and spatial spread of the ions. This independence is responsible for the high-resolution and mass accuracy of the Orbitrap [24–26].

Recently, Hu et al. developed a mass-selective method to manipulate ion populations in the Orbitrap by applying a resonant dipolar AC signal to the outer electrodes to excite or de-excite axial motion [31–33]. Excitation to larger amplitude ion axial motion is observed when the waveform is applied in phase with ion motion, whereas de-excitation to small (or even no) axial amplitude occurs if the resonant waveform is applied 180° out of phase with ion motion. The extent of ion axial excitation or de-excitation depends on the AC amplitude and on the number of cycles applied. By choosing the parameters appropriately, it is possible to mass-selectively eject ions or de-excite ions such that their signal cannot be observed above baseline noise. Using a phase enhanced technique, Hu et al. demonstrated high-resolution (28,000) mass selective ejection of ions [31]. After de-excitation, the ions continue to orbit the central electrode at the equator of the Orbitrap ($z = 0$). They could then be coherently re-excited by application of a second AC waveform, allowing their signal to be observed again. Similar techniques have been previously used to mass-selectively excite, de-excite, and eject ions in FT-ICR MS [34, 35].

The ability to manipulate confined ion populations provides the potential for performing ion activation and MS/MS inside the Orbitrap as opposed to hybrid instrument configurations that use external ion traps (such as the linear ion trap, C-trap, and octapole collision cell) [1, 3] for CID. Advantages of such an approach include (1) the possibility of bringing the Orbitrap's high mass accuracy and resolution to bear on both the precursor and product ions in the same MS/MS scan, and (2) making available the collision energy regime of the Orbitrap, ~1500 eV, not used in current types of instruments. These ion motion control techniques also allow for a wider range of experiments such as interrogating the dynamics of confined ion packets.

During the course of previous ion motion control experiments in this laboratory [31–33], it was observed that axial de-excitation of an ion population to the center of the Orbitrap ($z = 0$), followed by immediate re-excitation, produced mass spectral peaks that were narrower, more symmetric, and of equal or greater height than obtained from a regular mass spectrum using otherwise identical conditions. To investigate these effects, the injection optics were tuned to optimize peak shape and signal magnitude for a given analyte concentration. Then, by varying the compensator potential, conditions were found that reproducibly produced broad and multiply split peaks in regular mass spectra.

In this paper, we demonstrate that de-excitation of the ion population followed by immediate re-excitation—a process we term "rephasing"—can be employed to improve the peak shape and resolution of ion peaks in the Orbitrap mass analyzer. These performance parameters can be improved under both optimized and unoptimized ion injection and field compensator conditions. Although the prototype instrument [25] used for these experiments has different ion injection optics and a smaller Orbitrap than the commercial LTQ-Orbitrap, we believe that these results are of general interest, as they demonstrate that unoptimized injection conditions and deleterious space-charge effects may be compensated by ion motion control regimes in the Orbitrap analyzer [36].

Experimental

Materials

All chemicals were of the highest available purity and were used without further processing. For the experiments in which peak shapes and resolution were assessed as a function of reserpine (Sigma-Aldrich, St. Louis, MO) concentration, two sets of solutions were tested: 0.01 ng/μL to 1000 ng/μL and 0.1 ng/μL to 1000 ng/μL (referred to henceforth as datasets 1 and 2, respectively). All solutions were made by dissolution in methanol:water (50:50 vol%:vol%) with 0.1% (vol%) acetic acid and infused into the mass spectrometer at 5 μL/min using a syringe pump (Harvard Apparatus, model 22; South Natick, MA).

Orbitrap Mass Spectrometer

In this study, a prototype Orbitrap instrument built by Thermo Masslab Ltd. (Manchester, U.K.) was used and is described in detail elsewhere [24, 25]. Briefly, ions generated by an electrospray ionization (ESI) source (spray voltage = 3 kV) are drawn into a double-orthogonal inlet and transported through a radio frequency (rf)-only guide quadrupole (2.5 MHz, 0.1–1 kV_{p-p}, ~10^{-5} mbar). The ions then progress into a transport quadrupole (920 kHz, ~300 V_{p-p}), which brings the ions through several stages of pumping into

a linear quadrupole ion trap (3.45 MHz, 4100–4400 V_{p-p}) or "storage quadrupole," in which the N_2 pressure is $\sim 10^{-3}$ mbar. A ring electrode around the end of the storage quadrupole closer to the Orbitrap was set to 750 V to create an axial potential well. Collisions with the bath gas cause ions to lose kinetic energy and accumulate in the well.

Ions are accumulated for 400 ms and then are energized to 1330 eV by increasing the DC offset potential of the storage quadrupole. The exit gate is then pulsed open and the bunched ions are rapidly accelerated towards the Orbitrap, where the outer electrodes are maintained at virtual ground. A deflector/compensator electrode (Figure 1) deflects the extracted ion packet into the Orbitrap through a small opening in one of the outer electrodes [24, 26]. The deflector potential is held at 85 V during injection and is switched to 560 V during signal detection to minimize electric field perturbations inside the Orbitrap caused by the ion injection slot. During ion injection, the potential on the central electrode increases in magnitude, to ensure that the ions are radially trapped. During mass analysis and ion manipulation, the central electrode voltage is held constant at approximately −3400 V. Under unoptimized conditions, ions were energized to 1350 eV but, most importantly, the compensator potential was adjusted to 540 V to increase the anharmonicity that the ions would experience in the Orbitrap during mass analysis. All the other settings were kept the same.

Although the injection optics of this prototype differs from the commercial LTQ-Orbitrap and are more susceptible to space-charge effects [1], both systems produce ion packets with small temporal and spatial widths (few millimeters), important for high-performance analysis [26]. In addition, the Orbitrap analyzer in this prototype is smaller in diameter than the commercially available instrument, 8 mm inner electrode and 20 mm outer electrode, versus 12 mm and 30 mm, respectively [1, 26], although the instrument has comparable performance.

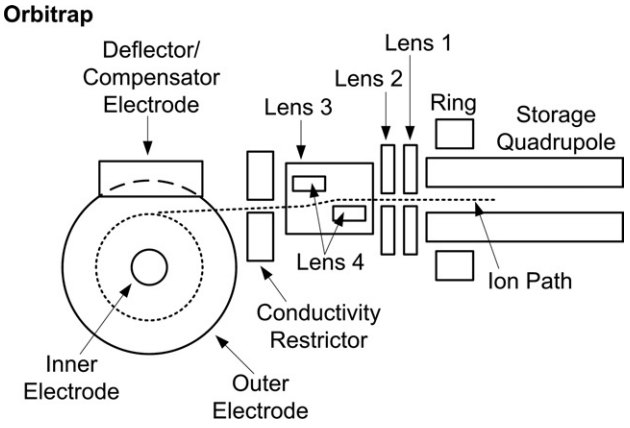

Figure 1. Schematic depiction showing the injection optics and deflector/compensator electrode of the prototype Orbitrap instrument. The dotted trace shows the ion path.

Rephasing

Injecting ions into the Orbitrap at a position offset from $z = 0$ gives the ions axial potential energy and ions of each m/z will begin coherent axial oscillation [26]. In all the experiments reported here, the monoisotopic peak of protonated reserpine (m/z 609) was used to assess the peak shape and resolution before and after rephasing. To rephase the ions, a resonant dipolar AC signal (447.2 kHz, 3.8 V_{p-p},) was applied to the split outer electrode using an arbitrary waveform generator (model AWG 420; Sony Tektronix, Richardson, TX). The number of cycles applied was adjusted to obtain the best improvement in performance and found to be in the range of 400–470 cycles. A digital delay generator (model DG535; Stanford Research Systems, Sunnyvale, CA) controlled timing and sequence of events in the experiment. The AC signal was applied 80 ms after opening the exit gate of the storage quadrupole. This delay is to allow complete radial and angular dephasing of the ion packet; acquisition of the transient started 40 ms later. The phase relationship of the AC relative to ion axial motion was set by adjusting the exact starting time of the AC waveform, precise to 100 ns, with the digital delay generator.

Fourier Transform

A sampling frequency of 5000 kHz was used. Transients of 2^{22} data points were acquired for all experiments. Transients were fast Fourier transformed using the MIDAS data analysis program [30] into a mass (or frequency) spectrum with no apodization and 2 zero fills. As a check, regular ("passive") and rephased mass spectra (1 ng/μL sample, from dataset 1) were processed using 1, 2, or 3 zero fills. No significant differences in peak shape, resolution ($R_{rephased}/R_{passive}$ = 3.4, 3.2, 3.1, respectively), peak area ($A_{rephased}/A_{passive}$ = 1.3, 1.4, 1.4, respectively), and peak magnitude ($P_{rephased}/P_{passive}$ = 2.7 for all cases) were observed, indicating that improvements in performance are due to rephasing. Data files for mass spectra (frequency, m/z and abundance values) were exported from MIDAS into Microsoft Excel, which was then used to calculate (1) peak areas by numerical integration, and (2) m/z resolving power (R) at full width at half maximum (FWHM) using the relation $R = 0.5(f/\Delta f) = m/\Delta m$, where Δf and Δm represent peak widths (FWHM) in the frequency and m/z domains, respectively. From this point forward the term "resolution" refers to the m/z domain.

Results

When the compensator voltage is detuned, the Orbitrap potential is anharmonic, resulting in broad mass spectral peaks. Traces representing five spectra, each acquired as a single transient, are shown in Figure 2 for 1 ng/μL and 10 ng/μL reserpine solutions. The passive spectra for the 1 ng/μL sample contain broad, multiply-

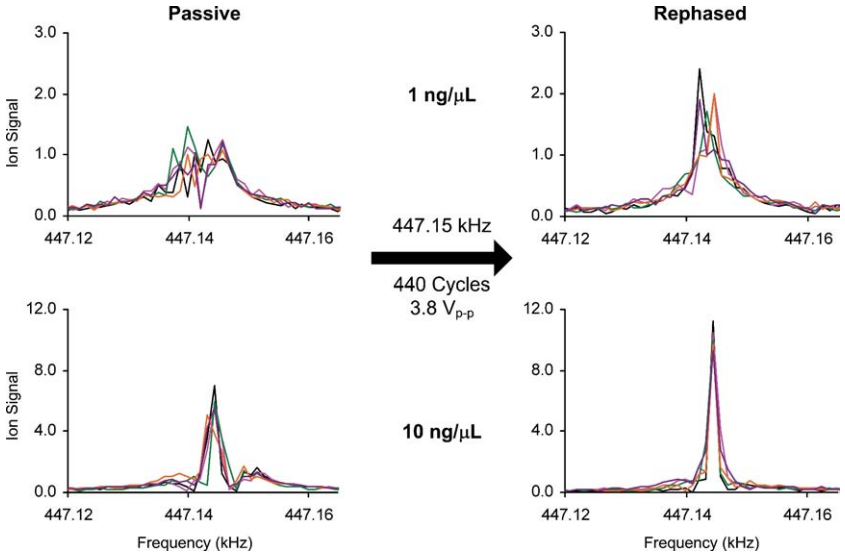

Figure 2. Passive (normal, left hand plots) and rephased (de-excited and immediately re-excited, right hand plots) mass spectra obtained for unoptimized injection and compensator settings for reserpine concentrations at 1 ng/μL (top plots) and 10 ng/μL (bottom plots). Each trace is a Fourier transform of a transient obtained from a single scan.

split peaks, indicating that the ion packet had a large frequency distribution (~20 Hz at FWHM). This results in a lowered resolution of R_p = 22,000 ("p", i.e., no application of AC waveform). All data in this paper are averages of at least three experimental determinations. Confidence limits (95%) are reported in the tables and also in the text where the authors wish to provide special emphasis. It is important to note that for all experiments, passive and rephased spectra were acquired sequentially, and therefore represent two different ion populations. After rephasing, R_r = 61,000 ("r" subscript denotes rephased mass spectrum), a 2.7-fold increase in resolution. The resolution and the height of the rephased peaks, R_r, and P_r, are significantly greater than the corresponding values of R_p, P_p obtained in the passive spectra. However, peak area, A_p and A_r, appears roughly conserved under our conditions. Table 1 gathers the numerical results using unoptimized injection/compensator conditions for reserpine concentrations of 1 ng/μL and 10 ng/μL.

For the 10 ng/μL sample, the peaks are split into three distinct lobes (Figure 2). Comparing the passive and rephased spectra for the 10 ng/μL sample in Figure 2, the peak shapes are significantly improved upon rephasing, with the side lobes disappearing and the ion distribution becoming more symmetrical about the cen-

Table 1. Peak height, peak area, and resolution for unoptimized ion injection conditions[a]

	1 ng/μL						10 ng/μL					
	Passive			Rephased			Passive			Rephased		
Spectrum	P_p[b]	A_p[c]	R_p[d]	P_r[b]	A_r[c]	R_r[d]	P_p[b]	A_p[c]	R_p[d,e]	P_r[b]	A_r[c]	R_r[d]
1	1.21	10.14	22,700	2.35	11.04	64,100	6.96	22.27	62,100	11.16	17.45	169,200
2	1.15	11.24	21,000	1.92	10.83	55,400	5.58	23.84	55,900	10.44	22.30	145,000
3	1.36	11.91	21,000	1.66	10.54	62,800	5.85	23.91	55,900	9.96	18.64	141,700
4	1.01	10.74	24,400	1.93	11.20	67,700	5.06	25.44	40,600	9.48	20.47	164,700
5	1.15	10.94	21,400	1.85	11.80	53,000	5.49	23.20	49,700	9.29	23.97	135,400
Average	1.2	11.0	22,000	1.9	11.1	61,000	5.8	23.7	53,000	10.1	20.6	151,000
95% CI[f]	0.1	0.7	1,000	0.3	0.5	6,000	0.7	1.2	8,100	0.8	2.6	15,000
R_r/R_p			2.7 ± 0.3						2.9 ± 0.5			
P_r/P_p			1.6 ± 0.3						1.7 ± 0.3			
A_r/A_p			1.01 ± 0.07						0.87 ± 0.12			

[a]Subscript p denotes passive mass spectrum; subscript r denotes rephased mass spectrum.
[b]Peak height.
[c]Peak area.
[d]Mass resolution.
[e]Resolution obtained from fitted Lorentzian taking account of side lobes; see text.
[f]CI: confidence interval.

Table 2. Peak height, peak area, and resolution for optimized ion injection conditions[a]

	1 ng/μL						10 ng/μL					
	Passive			Rephased			Passive			Rephased		
Spectrum	P_p[b]	A_p[c]	R_p[d]	P_r[b]	A_r[c]	R_r[d]	P_p[b]	A_p[c]	R_p[d]	P_r[b]	A_r[c]	R_r[d]
1	5.85	31.13	83,000	6.13	18.91	143,700	15.41	67.44	82,300	22.37	68.32	134,800
2	4.88	23.51	78,700	5.81	24.76	121,800	18.19	88.66	80,700	22.28	61.78	171,100
3	4.19	24.42	75,200	6.44	24.22	138,500	16.26	72.07	87,000	25.11	67.56	123,800
4	5.66	27.57	93,700	6.86	34.44	99,900	16.39	82.14	81,200	25.11	65.56	133,000
5	5.84	29.18	79,100	5.33	23.23	124,300	20.78	66.16	82,700	28.81	84.04	140,400
Average	5.3	27.2	82,000[a]	6.1	25.1	126,000[a]	17.4	75.3	83,000[a]	24.7	69.5	141,000[a]
95% CI[e]	0.7	3.2	7,000[a]	0.6	5.7	17,000[a]	2.1	9.8	2,000[a]	2.7	8.5	18,000[a]
R_r/R_p			1.5 ± 0.2						1.7 ± 0.2			
P_r/P_p			1.2 ± 0.2						1.4 ± 0.2			
A_r/A_p			0.92 ± 0.24						0.92 ± 0.16			

[a]Subscript p denotes passive mass spectrum; subscript r denotes rephased mass spectrum.
[b]Peak height.
[c]Peak area.
[d]Mass resolution.
[e]CI: confidence interval.

tral m/z value. For the passive spectra, the width of the central lobe, considered alone, would yield $R_p = 89{,}000$. However, this would not account for the prominent side lobes. Therefore, to obtain an accurate estimate for R_r/R_p for the 10 ng/μL samples, the passive mass spectral peaks were fitted to a Lorentzian of form $\Delta f[a(f-f_o)^2+(\Delta f/2)^2]^{-1}$, where f_o is the central frequency, Δf is the FWHM and a is a constant [37]. The fit was adjusted to match the experimentally measured area for all three lobes while keeping the magnitude at f_o constant. The resulting fit was thus a compromise: wider than the central lobe but not completely encompassing the side lobes. Using this method, a value of $R_p = 53{,}000$ is measured and R_r/R_p is calculated to be 2.9, consistent with the improvement in resolution obtained for the 1 ng/μL sample (Table 1).

For the 1 and 10 ng/μL samples, peak area appears conserved upon rephasing (A_r/A_p = 1.01 and 0.87, respectively), but peak height (P) shows a small increase of 1.6 and 1.7, (Table 1). Thus, rephasing appears to produce an ion packet with a narrower frequency distribution and, presumably, narrower axial distribution (i.e., higher resolution and magnitude) that is more symmetric about a central frequency. Additionally, as peak area is proportional to the number of ions in the packet as well as their axial amplitude (eq 3), two cases are possible during rephasing: either (1) few ions are lost and that their rephased z-amplitudes are roughly equal to their original z-amplitudes, or (2) ions are lost but that the rephased z-amplitudes of the remaining ions are greater than their original z-amplitudes. Previous ion motion control experiments (albeit under ideal conditions) [32] and simulations (which did not take ion-ion interactions into account) [33] suggest that de-excitation and re-excitation each take the same number of cycles of AC, indicating that case (1) is more likely.

The ion injection optics can affect the ion packets' widths and exact locations in the Orbitrap upon injection and thus can conceivably affect resolution, mass accuracy and sensitivity. Therefore, analogous experiments were conducted for optimized ion injection/compensator parameters; the data in Table 2 thus constitute "comparison" data, acquired at the same time as those in Table 1. For 1 ng/μL, the resolution in passive spectra (R_p) was 82,000, whereas R_r was improved to 126,000. The 10 ng/μL sample showed a similar increase in resolution from 83,000 to 141,000. Table 2 shows that peak area is approximately conserved, $A_r/A_p = 0.92$ for both 1 and 10 ng/μL samples. Meanwhile, there was a small increase in peak height, $P_r/P_p = 1.2 \pm 0.2$ and 1.4 ± 0.2, respectively, for 1 and 10 ng/μL. These results suggest that even with optimized injection parameters, rephasing increases performance without any significant loss in ion signal.

Additionally, exact values for tuning of injection lens potentials also depend upon ion densities in the injected ion beam. Therefore, additional experiments were carried out to determine the effectiveness of rephasing as a function of analyte concentration under injection conditions optimized at an intermediate concentration. Two additional separate datasets, with concentration ranges of 0.01–1000 ng/μL and 0.1–1000 ng/μL, were acquired on different days. On each day, injection parameters were initially (and separately) optimized for the 10 ng/μL samples. Then, passive and rephased spectra were recorded for each sample in increasing order of concentration. Whereas the commercial LTQ-Orbitrap instrument uses the automatic gain control (AGC) [38] feature of the first stage linear ion trap mass analyzer to regulate the number of ions injected into the Orbitrap, thereby minimizing the dependence of Orbitrap performance on ion concentration, the prototype Orbitrap instrument used here does not have this capability.

The ratio R_r/R_p, indicating improvement upon rephasing, rapidly decreases to unity at 10 ng/μL for

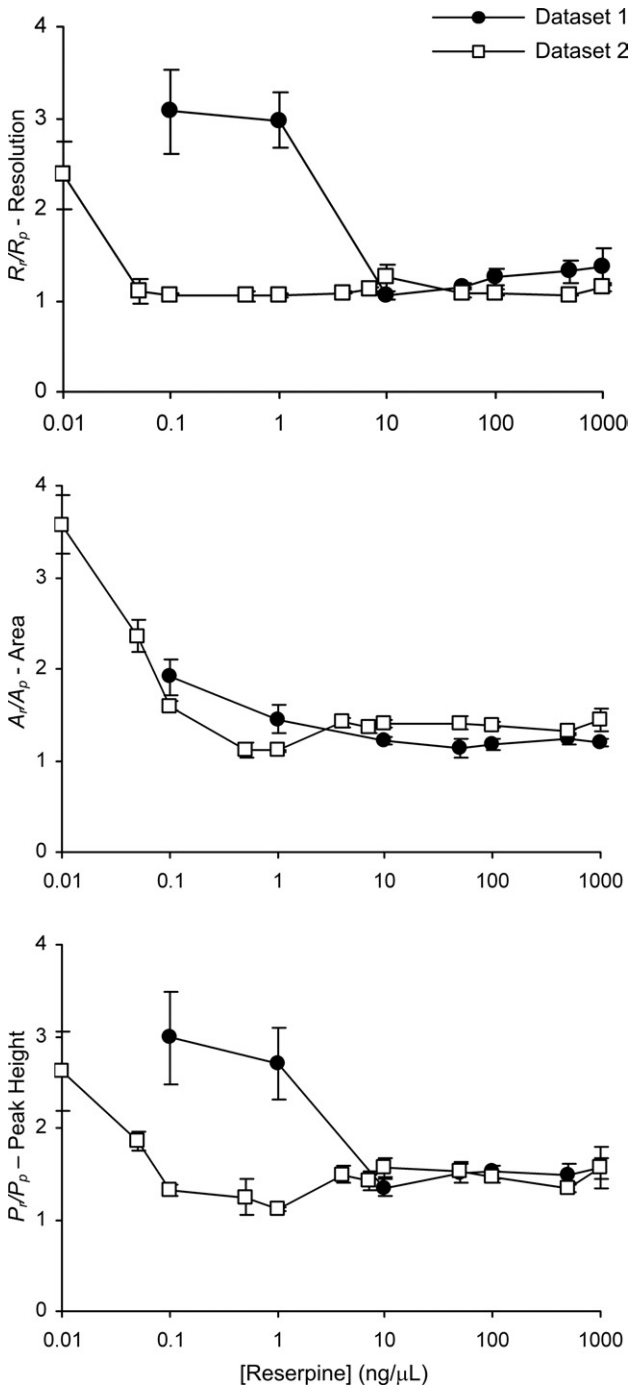

Figure 3. Plots showing changes in resolution (R_r/R_p), peak area (A_r/A_p), and peak magnitude (P_r/P_p) upon rephasing as a function of solution concentration for datasets 1 and 2. Experimental conditions optimized at 10 ng/μL

dataset 1 and 0.05 ng/μL for dataset 2 (Figure 3). For concentrations at which $R_r/R_p \approx 1$, the average R_p is 121,000 ± 12,000 (10 ng/μL to 1000 ng/μL) for dataset 1 and 138,000 ± 8000 (0.05 ng/μL to 1000 ng/μL) for dataset 2. The average for R_r is 148,000 ± 2000 and 152,000 ± 3000, respectively. The greatest improvement in resolution was observed in dataset 1 for the 0.1 ng/μL and 1 ng/μL samples, increasing from 32,300 ± 1000 to 99,000 ± 14,000 (R_r/R_p = 3.1 ± 0.5) and 48,000 ± 3000 to 142,000 ± 12,000 (R_r/R_p = 3.0 ± 0.3). R_r/R_p for the 0.01 ng/μL sample (dataset 2) is 2.4 ± 0.4, increasing from 39,000 ± 6000 to 92,000 ± 1000. For higher concentrations in dataset 2, the improvement in resolution was small but possibly significant, with an average R_r/R_p of 1.23 ± 0.10 over this range. In dataset 2, R_r/R_p has the largest value (2.38 ± 0.15) at 0.01 ng/μL (Figure 3). For all other points, the average improvement in resolution was 1.10 ± 0.05. These observations indicate that the optimized injection parameters used to acquire dataset 2 (ring and injection lens potentials, optimized daily) produced ion packets in the Orbitrap that had narrower frequency and axial distributions over a wider range of concentrations, compared with the settings used for dataset 1.

The 2- to 3-fold increase in resolution upon rephasing observed for low analyte concentrations suggests that the ion injection conditions are better for larger numbers of ions. There is an increase in both peak area and height for datasets 1 and 2 after rephasing at low concentration (0.01 and 0.05 ng/μL). The increase in peak area suggests that ions of a given m/z may have been excited to larger axial amplitudes.

Rephasing can be understood by invoking simple arguments regarding the nature of the one-dimensional axial potential, taking into account anharmonic terms as well as ion–ion interactions. A nonoptimal compensator voltage and truncation of the electrodes will introduce third and fourth order anharmonic terms into the axial potential. Upon differentiation, these appear as square and cubic terms in the equation of motion:

$$\ddot{z} + \omega^2 z + \alpha z^2 + \beta z^3 = 0 \quad (4)$$

Using the method of successive approximations, the axial frequency of the ion is given by

$$\omega = \omega_0 + \left(\frac{3\beta}{8\omega_0} - \frac{5\alpha^2}{12\omega_0^3}\right)(\Delta z)^2 \quad (5)$$

where $\omega_o = (kq/m)^{1/2}$ is the natural (harmonic) frequency of the ion and Δz is the axial amplitude of the ion [39]. Similar relationships have been described for Paul [40] and FT-ICR [41] traps.

Equation 5 illustrates that in an anharmonic potential, the frequency of an ion depends on its amplitude (Δz, which is determined by the initial position upon injection) and the magnitude of anharmonicity (α and β). So, when the compensator electrode value is not optimal, the greater anharmonicity produces spectra with a broader frequency distribution, Δf = 20 Hz (FWHM), yielding R_p of 22,000 (Table 1 and Figure 2), compared with spectra acquired under optimum conditions, Δf = 3 Hz (FWHM), R_p of 82,000 (Table 2) when the magnitude of α is small.

When an AC de-excitation waveform is applied to the outer electrodes, the axial amplitude and axial kinetic energy of the ions are decreased until the ion

packet's axial motion is stopped (or nearly so) and the ions confined to the equatorial plane ($z = 0$) of the Orbitrap. Since the bandwidth of the AC is large (~2000 Hz) compared to the frequency distribution of the ions, all ions in the packet suffer de-excitation. After de-excitation to $z = 0$, further application of the AC coherently re-excites the ions to a new amplitude. In our experiment, the end effect is to produce a re-excited ion packet that has a smaller axial width and narrower frequency distribution (i.e., higher packet coherency) compared with the packet's initial distribution that was formed during injection. During the time that the ions are compressed into a smaller axial extent, increased space charge interactions cause their velocities (and hence axial frequencies and kinetic energies) to average or "thermalize," thereby reducing the width of the frequency distribution. This phenomenon is well-known; similar space charge-induced frequency shifts and indeed, coalescence of closely neighboring peaks, have been observed in FT-ICR [42, 43] and QIT [44, 45] MS.

Rephasing may also be of considerable utility, as it offers the possibility that Orbitrap performance need not depend as strongly or as critically upon the exact details of ion injection into the Orbitrap. Future work will include ion optical modeling to gain additional insight into details of the rephasing mechanism.

Acknowledgments

The authors acknowledge the National Science Foundation MRI program 0216239-CHE and Office of Naval Research N00014-05-0454 for support, as well as Jason S. Duncan for his expertise in electrical engineering.

References

1. Makarov, A.; Denisov, E.; Kholomeev, A.; Balschun, W.; Lange, O.; Strupat, K.; Horning, S. Performance evaluation of a hybrid linear ion trap/Orbitrap mass spectrometer. *Anal. Chem.* **2006,** *78,* 2113–2120.
2. Olsen, J. V.; de Godoy, L. M. F.; Li, G.; Macek, B.; Mortensen, P.; Pesch, R.; Makarov, A. A.; Lange, O.; Horning, S.; Mann, M. Parts per million mass accuracy on an Orbitrap mass spectrometer via lock mass injection into a C-trap. *Mol. Cell. Proteom.* **2005,** *4,* 2010–2021.
3. Olsen, J. V.; Macek, B.; Lange, O.; Makarov, A. A.; Horning, S.; Mann, M. Higher-energy C-trap dissociation for peptide modification analysis. *Nature Methods* **2007,** *4,* 709–712.
4. Perry, R. H.; Cooks, R. G.; Noll, R. J. Orbitrap mass spectrometry: Instrumentation, ion motion, and applications. *Mass Spectrom. Rev.* **2008,** *27,* 661–699.
5. Makarov, A. A.; Denisov, E.; Lange, O.; Horning, S. Dynamic range of mass accuracy in LTQ Orbitrap hybrid mass spectrometer. *J. Am. Soc. Mass Spectrom.* **2006,** *17,* 977–982.
6. Aebersold, R.; Mann, M. Mass spectrometry-based proteomics. *Nature* **2003,** *422,* 198–207.
7. Henzel, W. J.; Billeci, T. M.; Stults, J. T.; Wong, S. C.; Grimley, C.; Watanabe, C. Identifying proteins from two dimensional gels by molecular mass searching of peptide fragments in protein sequence databases. *Proc. Natl. Acad. Sci. U.S.A.* **1993,** *90,* 5011–5015.
8. Wilm, M.; Shevchenko, A.; Houthaeve, T.; Breit, S.; Schweigerer, L.; Fotsis, T.; Mann, M. Femtomole sequencing of proteins from polyacrylamide gels by nano-electrospray mass spectrometry. *Nature* **1996,** *379,* 466–469.
9. Li, X.; Gerber, S. A.; Rudner, A. D.; Beausoleil, S. A.; Haas, W.; Villén, J.; Elias, J. E.; Gygi, S. P. Large-scale phosphorylation analysis of alpha-factor-arrested. *Saccharomyces cerevisiae. J. Proteome. Res.* **2007,** *6,* 1190–1197.
10. Yates, J. R.; Cociorva, D.; Liao, L.; Zabrouskov, V. Performance of a linear ion trap-Orbitrap hybrid for peptide analysis. *Anal. Chem.* **2006,** *78,* 493–500.
11. Aebersold, R.; Goodlett, D. R. Mass spectrometry in proteomics. *Chem. Rev.* **2001,** *101,* 269–295.
12. Hunt, D. F.; Yates, J. R.; Shabanowitz, J.; Winston, S.; Hauer, C. R. Protein sequencing by tandem mass spectrometry. *Proc. Natl. Acad. Sci. U.S.A.* **1986,** *83,* 6233–6237.
13. Frank, A. M.; Savitski, M. M.; Nielsen, M. L.; Zubarev, R. A.; Pevzner, P. A. De novo peptide sequencing and identification with precision mass spectrometry. *J. Proteome Res.* **2007,** *6,* 114–123.
14. Scigelova, M.; Makarov, A. Orbitrap mass analyzer - Overview and applications in proteomics. *Proteomics* **2006,** *6,* 16–21.
15. Macek, B.; Waanders, L. F.; Olsen, J. V.; Mann, M. Top-down protein sequencing and MS^3 on a hybrid linear quadrupole ion trap-Orbitrap mass spectrometer. *Mol. Cell. Proteom.* **2006,** *5,* 949–958.
16. Thevis, M.; Bredehöft, M.; Geyer, H.; Kamber, M.; Delahaut, P.; Schänzer, W. Determination of Synacthen in human plasma using immunoaffinity purification and liquid chromatography/tandem mass spectrometry. *Rapid Commun. Mass Spectrom.* **2006,** *20,* 3551–3556.
17. Zhang, Z.; Shah, B. Characterization of variable regions of monoclonal antibodies by top-down mass spectrometry. *Anal. Chem.* **2007,** *79,* 5723–5729.
18. Ge, Y.; Lawhorn, B. G.; El Naggar, M.; Strauss, E.; Park, J.-H.; Begley, T. P.; McLafferty, F. W. Top down characterization of larger proteins (45 kDa) by electron capture dissociation mass spectrometry. *J. Am. Chem. Soc.* **2002,** *124,* 672–678.
19. Kelleher, N. L.; Lin, H. Y.; Valaskovic, G. A.; Aaserud, D. J.; Fridriksson, E. K.; McLafferty, F. W. Top-down versus bottom-up protein characterization by tandem high-resolution mass spectrometry. *J. Am. Chem. Soc.* **1999,** *121,* 806–812.
20. Sze, A. K.; Ge, Y.; Oh, H.; McLafferty, F. W. Top-down mass spectrometry of a 29-kDa protein for characterization of any posttranslational modification to within one residue. *Proc. Natl. Acad. Sci. U.S.A.* **2002,** *99,* 1774–1779.
21. Peterman, A. M.; Duczak Jr., N.; Kalgutkar, A. S.; Lame, M. E.; Soglia, J. R. Application of a linear ion trap/Orbitrap mass spectrometer in metabolite characterization studies: Examination of the human liver microsomal metabolism of the non-tricyclic anti-depressant nefazodone using data-dependent accurate mass measurements. *J. Am. Soc. Mass Spectrom.* **2006,** *17,* 363–375.
22. Ejsing, C. S.; Moehring, T.; Bahr, U.; Duchoslav, E.; Karas, M.; Simons, K.; Shevchenko, A. Collision-induced dissociation pathways of yeast sphingolipids and their molecular profiling in total lipid extracts: A study by quadrupole TOF and linear ion trap-Orbitrap mass spectrometry. *J. Mass Spectrom.* **2006,** *41,* 372–389.
23. Barceló, D.; Petrovic, M. Challenges and achievements of LC-MS in environmental analysis: 25 years on. *Trends Anal. Chem.* **2007,** *26,* 2–11.
24. Hardman, M.; Makarov, A. A. Interfacing the Orbitrap mass analyzer to an electrospray ion source. *Anal. Chem.* **2003,** *75,* 1699–1705.
25. Hu, Q.; Noll, R. J.; Li, H. Y.; Makarov, A.; Hardman, M.; Cooks, R. G. The Orbitrap: A new mass spectrometer. *J. Mass Spectrom.* **2005,** *40,* 430–443.
26. Makarov, A. Electrostatic axially harmonic orbital trapping: A high-performance technique of mass analysis. *Anal. Chem.* **2000,** *72,* 1156–1162.
27. Brigham, E. O. The Fast Fourier Transform; Prentice-Hall: Englewood Cliffs, NJ, 1974.
28. Champeney, D. C. Fourier Transforms and their Physical Applications; Academic Press: New York, NY, 1973.
29. Bracewell, R. *The Fourier Transform and Its Applications* 3rd ed; McGraw Hill: Boston, MA, 2000.
30. Senko, M. W.; Canterbury, J. D.; Guan, S.; Marshall, A. G. A high-performance modular data system for Fourier transform ion cyclotron resonance mass spectrometry. *Rapid Commun. Mass Spectrom.* **1996,** *10,* 1839–1844.
31. Hu, Q.; Cooks, R. G.; Noll, R. J. Phase-enhanced selective ion ejection in an Orbitrap mass spectrometer. *J. Am. Soc. Mass Spectrom.* **2007,** *18,* 980–983.
32. Hu, Q.; Makarov, A. A.; Cooks, R. G.; Noll, R. J. Resonant AC dipolar excitation for ion motion control in the Orbitrap mass analyzer. *J. Phys. Chem. A* **2006,** *110,* 2682–2689.
33. Wu, G.; Noll, R. J.; Plass, W. R.; Hu, Q.; Perry, R. H.; Cooks, R. G. Ion trajectory simulations of axial AC dipolar excitation in the Orbitrap. *Int. J. Mass Spectrom.* **2006,** *254,* 53–62.
34. Chen, L.; Marshall, A. G. Stored waveform simultaneous mass-selective ejection/excitation for Fourier transform ion cyclotron resonance mass spectrometry. *Int. J. Mass Spectrom. Ion Processes* **1987,** *79,* 115–125.
35. Marshall, A. G.; Wang, T.-C. L.; Ricca, T. L. Ion cyclotron resonance excitation/de-excitation: A basis for stochastic Fourier transform ion cyclotron mass spectrometry. *Chem. Phys. Lett.* **1984,** *105,* 233–236.
36. Kaiser, N. K.; Bruce, J. E. Observation of increased ion cyclotron resonance signal duration through electric field perturbations. *Anal. Chem.* **2005,** *77,* 5973–5981.
37. Gough, W. The graphical analysis of a Lorentzian function and a differentiated Lorentzian function. *J. Phys. A* **1968,** *1,* 704–709.
38. Schwartz, J. C.; Zhou, X. G.; Bier, M. E. *Method and apparatus of increasing dynamic range and sensitivity of a mass spectrometer*, U.S. Patent 5,572,022, 1995.
39. Landau, L. D.; Lifshitz, E. M. Mechanics; Pergamon Press: Oxford, NY, 1976.
40. Sevugarajan, S.; Menon, A. G. Frequency perturbation in nonlinear Paul traps: A simulation study of the effect of geometric aberration, space

charge, dipolar excitation, and damping on ion axial secular frequency. *Int. J. Mass Spectrom.* **2000,** *197,* 263–278.
41. Mitchell, D. W.; Rockwood, A. L.; Smith, R. D. Frequency shifts and modulation effects due to solenoidal magnetic field inhomogeneities in ion cyclotron mass spectrometry. *Int. J. Mass Spectrom. Ion Processes* **1995,** *141,* 101–116.
42. Jeffries, J. B.; Barlow, S. E.; Dunn, G. H. Theory of space-charge shift of ion cyclotron resonance frequencies. *Int. J. Mass Spectrom. Ion Processes* **1983,** *54,* 167–187.
43. Huang, J.; Tiedemann, P. W.; Land, D. P.; McIver, R. T.; Hemminger, J. C. Dynamics of ion coupling in a FTMS ion trap and resulting effects on mass spectra, including isotope ratios. *Int. J. Mass Spectrom. Ion Processes* **1994,** *134,* 11–21.
44. Jungmann, K.; Hoffnagle, J.; DeVoe, R. G.; Brewer, R. G. Collective oscillations of stored ions. *Phys. Rev. A At. Mol. Opt. Phys.* **1987,** *36,* 3451–3454.
45. Mo, W.; Todd, J. F. J. Investigation of the mass shifts caused by the coupling of ion motions in the ion trap mass spectrometer. *Rapid Commun. Mass Spectrom.* **1996,** *10,* 424–428.